Transplantation of Nanostructured Composite Scaffolds Results in the Regeneration of Chronically Injured Spinal Cords

ARTICLE *in* ACS NANO · JANUARY 2011

Impact Factor: 12.88 · DOI: 10.1021/nn102461w · Source: PubMed

Transplantation of Nanostructured Composite Scaffolds Results in the Regeneration of Chronically Injured Spinal Cords

Fabrizio Gelain,[†,‡,*] Silvia Panseri,[†] Stefania Antonini,[†,‡] Carla Cunha,[†,‡] Matteo Donega,[†,‡] Joseph Lowery,[§] Francesca Taraballi,[†,‡] Gabriella Cerri,[⊥] Marcella Montagna,[⊥] Fausto Baldissera,[⊥] and Angelo Vescovi[†,‡,*]

[†]Biotechnology and Biosciences Department, University of Milan-Bicocca, Milan 20126, Italy, [‡]Center for Nanomedicine and Tissue Engineering - A.O. Niguarda Ca' Granda, Milan 20162, Italy, [§]Institute for Soldier Nanotechnologies, Massachusetts Institute of Technology, Cambridge, Massachusetts 02139, United States, and [⊥]Department of Human Physiology, University of Milan, Milan 20133, Italy

ABSTRACT The destruction and hollowing of entire tissue segments represent an insurmountable barrier to axonal regeneration and therapeutics in chronic spinal cord injury. To circumvent this problem, we engineered neural prosthetics, by assembling electrospun nanofibers and self-assembling peptides into composite guidance channels and transplanted them into the cysts of a postcontusive, chronic spinal cord injury rat model, also providing delivery of proregenerative cytokines. Six months later conspicuous cord reconstruction was observed. The cyst was replaced by newly formed tissue comprising neural and stromal cells. Nerve fibers were interspersed between and inside the guidance channels, spanning the lesion, amidst a well-developed vascular network, basal lamina, and myelin. This was accompanied by a significant improvement in the activity of ascending and descending motor pathways and the global locomotion score. Thus by engineering nanostructured matrices into neuroprosthetics, it is possible to recreate an anatomical, structural, and histological framework, which leads to the replacement of large, hollow tissue gaps in the chronically injured spinal cord, fostering axonal regeneration and neurological recovery.

KEYWORDS: self-assembling peptide · spinal cord injury · tissue engineering · electrospinning · evoked potentials

A complex cascade of harmful events underlies the establishment of chronic spinal cord injury (SCI). The complexity of this cascade has been described in some detail, from the events following the initial contusion[1] to those establishing chronic injuries.[2] When developing treatments for SCI, the complexity of the task at hand varies with the stage of the lesion, peaking in chronic injuries. Key pathophysiological factors, such as lack of neurotrophic stimulation or permissive substrates,[3] inhibitory environment,[4] secondary inflammatory damage,[5] and intrinsic growth deficiency in adult neurons,[6] have been targeted with a good degree of success in acute and subacute SCI.[3,7] Unfortunately, despite significant progress, chronic injuries still present us with a complex scenario. Over time, damaged axons undergo atrophy,[8] retrograde degeneration and retraction,[9] while genes required for regeneration are down regulated.[10] This is compounded by the eventual establishment of a refractory barrier of extracellular matrix and glial scarring at the injury site.[7] Complementary approaches, including cell therapy,[11,12] digestion of glial scarring,[7,11] neurotrophic factor delivery,[13] and electrical stimulation of the tissue surrounding the injury site[14] as well as clinical rehabilitation,[15] are being developed to accomplish nerve fiber regeneration and functional restoration in SCI. Intriguingly, Schwann cell transplantation can produce partial recovery in subacute contusive lesions,[16] and effective bridging and functional improvements have recently been accomplished in chronic SCI by combinatorial approaches, modifying both neuronal-intrinsic and -extrinsic growth mechanisms[17] and exploiting neural progenitors transplantation.[18]

While the scenario is now turning on the brighter side, the breadth of destruction of the nervous tissue observed in chronic SCI in humans—with entire sections of the spinal cord being replaced by fluid-filled cysts—remains a critical concern. Within these regions, the mechanical substrates that provide physical support for axonal regeneration and three-dimensional positional information as well as the cytoarchitectural organization required for effective nerve regrowth have gone permanently lost. Hence, a most pressing issue in chronic SCI is to warrant a suitable level of

*Address correspondence to fabrizio.gelain@unimib.it, angelo.vescovi@unimib.it.

Received for review September 20, 2010 and accepted December 13, 2010.

10.1021/nn102461w

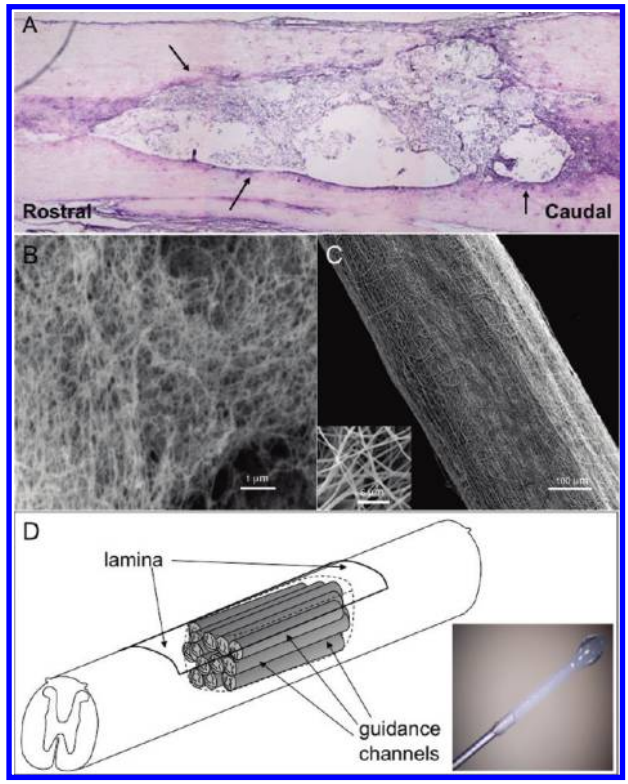

Figure 1. Injury model and scaffold preparation. (A) hematoxylin-eosin of a one-month old spinal cord lesion in longitudinal section; arrows point at the cyst margins containing tissue debris (magnification 5X). SEM images of self-assembled RADA16-I-BMHP1 (B) and of an electropsun, PCL/PLGA microguidance channel (C); a high-power magnification is shown in the inset. (D) Schematic representation of scaffold implantation. Conduits, presoaked in PBS and filled with RADA16-I-BMHP1 self-assembling peptide *via* microsyringe injection (inset), were placed singularly within the cavity following scar ablation. An electrospun lamina was sutured and glued to the meninges.

anatomical, histological, and cellular reconstruction at the lesion site. Thus, the scar tissue and hollow cysts should be replaced with new neural tissue, permissive for both axonal regrowth and lesion bridging. Pioneering studies on acute injuries show the usefulness of various artificial or biological materials in acute and subacute SCI.[19,20] In particular Teng and colleagues obtained significant functional recovery in poly(lactic-co-glycolic acid) (PLGA) scaffolds seeded with neural stem cells.[21] In animal models of complete transection, Bunge's group obtained significant axonal regeneration and myelination within implanted resorbable polymeric scaffolds seeded with Schwann cells.[22] Unfortunately, similar studies on chronicized contusions in the spinal cord, the most frequent situation in clinics, are few. Biomatrix bridges, mixed with cells of olfactory epithelial origin, were explored but failed to sustain chronically injured cortico-spinal axons.[23] Better results were obtained through the use of longitudinal channels within poly(ε-caprolactone) (PCL) foam implants, that supported axonal regrowth, albeit for a limited time.[24]

Self-assembling peptides (SAPs) and electrospun constructs, both characterized by their nanoscale architecture, are now being used in regenerative medicine,[25,26] including neuroregeneration[27,28] and slow delivery of cytokines.[29] Here we tackled the issue of anatomical and functional reconstruction in chronic SCI by using SAPs in a combinatorial approach, in which they were assembled into electrospun microchannel guidance constructs made of PLGA and PCL blended fibers. The aim was to establish a "neuro-prosthetic" which would improve directional axonal regeneration while supplying critical mechanical compliance, biocompatibility and degradation, and high porosity and functionalization with biologically active motifs.[30] These microconduits, alone or imbued with a mix of regenerative cytokines,[31,32] were transplanted into the large cysts that formed in the postcontusive spinal cord one month after injury. Six months later, we found that, while cysts persisted in control and sham-operated animals, they had been replaced by neo-formed tissue in animals transplanted with microconduits. The latter contained and was intermingled with bundles of regenerating axons and myelin, deposition of extracellular matrix (ECM) and stromal cells, and well developed neovascular structures, in the absence of considerable inflammatory response. This was matched by significant improvement in motor function on the Basso, Beattie, and Bresnahan (BBB) scale and in amplitudes and latencies of evoked responses in ascending tracts. Thus, transplantation of combined electrospun fibers/SAP scaffolds neuro-prosthetics supports broad anatomical and histological reconstruction and significant functional recovery in the chronically injured, hollowed spinal cord.

RESULTS

Surgery and Scaffold Implantation. We investigated a postcontusion, chronic SCI rat model characterized by centrally located cavities (cysts)[33] and surrounded by gliotic scar tissue, four weeks following a standardized, weight-drop trauma[34] (Figure 1A).

Various biological or synthetic materials have been proposed in order to develop therapies for the injured spinal cord,[19,20] although most attempts have focused on acute transection lesions rather than the postcontusion damage most frequent in humans.[35] These comprise the use of a combination of synthetic guidance channels, hydrogel fillers, growth factors, and fetal, schwann, or bone marrow cells in acute SC transection studies.[20,22,36,37]

Here, we attempted to reinstate an appropriate structural and environmental regenerative milieu using SAP-assembled tridimensional nanostructures (Figure 1B).

Using electrospinning, we generated hollow channels of nanofibers, composed of blended PCL and PLGA at a weight ratio of 5.5/4. The PLGA provides short-term strength, and the PCL provides long-term stability.[38] By this, we achieved a long-lasting reabsorption

time *in vivo* (over 6 months), while preserving fiber thickness and electrospun frame permeability. The average fiber diameter was 592 ± 225 nm and the tube length was between 2 and 3 mm, depending on the cavities to be filled. The outer tube diameter and wall thickness were 360 and 90 μm, respectively (Figure 1C and inset). Right before implantation guidance channels were wetted with phosphate buffer saline solution, infiltrating tubular walls and wetting their inner lumens due to capillary forces, which allowed for easy tube removal.

In this context, a key issue is that synthetic polymers, including those we used, lack cell adhesion sites, providing poor support for neural cells.[39] Furthermore, PCL is hydrophobic, similar to synthetic polymer nanofibers, in which the decrease in diameter increases the effective contact angle, making them unsuitable for neural cell growth and differentiation. Thus, although electrospinning can produce submicrometer, polymeric fibrous scaffolds, further modifications become necessary to establish an environment that will effectively support neural cell functions. Incorporation of neurite-promoting ECM proteins tissue in polymeric electrospun scaffolds has been proposed to mimic the native properties of the nervous tissue.[40] To do that, we assembled nanostructured SAPs scaffolds[30] at 1% (w/v) concentration within microstructured frames (a blend of PLGA and PCL), producing a novel kind of neuroprosthetics, shaped into longitudinal guidance microchannels, filled with functionalized SAP hydrogels, alone or combined with a mix of neurotrophic cytokines (Figure 1D).[31,32] Peptide self-assembly occurred inside the cavity of electrospun conduits, previously wetted with phosphate buffer saline solution (pH 7.4), filled by microsyringe injection (Figure 1D, inset), and was routinely verified (Figure S1, Supporting Information). Since it has been proven that matrices foster better neuronal growth when constructed with a compliance similar to nervous tissue,[41] we accordingly chose a SAP concentration of 1% (w/v) to yield a hydrogel scaffold stiffness similar to the spinal cord (unpublished experiments). The guidance effect exerted by the electrospun conduits was warranted in part by their mechanical stiffness, measured to be 1−2 orders of magnitude greater than SAP hydrogels (mechanical characterization tests unpublished).

Four weeks after the trauma, animals were assessed for BBB motor score and randomly divided in three experimental groups: sham operated, *i.e.*, rats subjected to the whole surgical procedure (including meninges incision and surgical scar debridement) but not receiving channel implants (group 0); rats implanted with guidance channels with RADA16-I-BMHP1[30] (RIB) alone (group 1); or loaded with brain-derived neurotrophic factor, ciliary neurotrophic factor, vascular endothelial growth factor, and chondroithinaseABC (RIB-GF) (group 2). Depending on the geometry of the cyst, 10−13 aligned tubes were implanted and oriented along the longitudinal spinal cord axis (Figure 1D). Spaces among the channels were filled with the matching RIB or RIB-GF SAP preparation. Lastly, an electrospun lamina (of identical chemical composition and similar fiber diameters to the guidance conduits) was sutured to the *dura mater* and sealed with fibrin glue.

Histological Findings and Perineural Tissue Regeneration. Seven months after the lesion (6 months after scar ablation and channel implantation) 5 animals in group 0 (33%), 4 in group 1 (25%), and 7 in group 2 (33%) had died due to postsurgical complications. At the same time ependymal canal disruption, dural fibrosis, and intraparenchymal cystic cavitation were observed in sham-operated animals (Figure 2A), compounded by injury to the dorsal corticospinal tract, gracile fasciculi, and postsynaptic dorsal column pathways.[42] Indeed the SC in sham-operated animals were characterized by cavities which filled a very large area of the cord section. On the contrary, the apparent SC anatomy was strikingly improved in animals implanted with guidance channels both in groups 1 and 2 (Figure 2B and C). Cavities were no longer present, and the whole spinal cord section was now made of new tissue, composed of morphologically distinct cells and interspersed in the interstitial spaces between the degrading guidance channels as well as inside their lumen (Figure 2B and C). Part of the ventral and lateral roots of the spinal cords was still present in all groups, as expected in this kind of lesion.[33]

The nature of the newly formed tissue in groups 1 and 2 was studied by confocal microscopy. Staining for laminin and collagen IV, two basic components of basement membranes in nervous tissues, was conspicuous and widespread (Figure 2D and E). Laminin deposits (green) surrounded NF200 positive fibers (red) (Figure 2D), whereas collagen IV (green) was located within the tissue regenerated throughout the microguidance channel inner lumen, evincing blood vessel morphology. Anti-CD68 immunolabeling revealed physiological numbers of macrophages inside the tubes lumen and, more frequently, in the degrading tube walls, consistent with the ongoing process of bioabsorption of the electrospun frames (Figure 2E). Interestingly, a well-developed vascular network was observed, both inside and between the guidance conduits. Blood vessel and small capillaries were found inside nearly all of the guidance tubes, within their walls and between them (Figure 2F and G arrows). It is worth noting that distribution and frequency of the blood vessels were reminiscent of healthy spinal cord tissue and that the neoangiogenesis unfolded preferentially along the longitudinal axes of the spinal cord and guidance tubes (Figure 2G). Similarly, fibroblasts were detected in the inner lumens and within the fiber meshes of the tubular walls (Figure 2F in green). Iba-1 positive, microglial cells were located inside the electrospun tubes at physi-

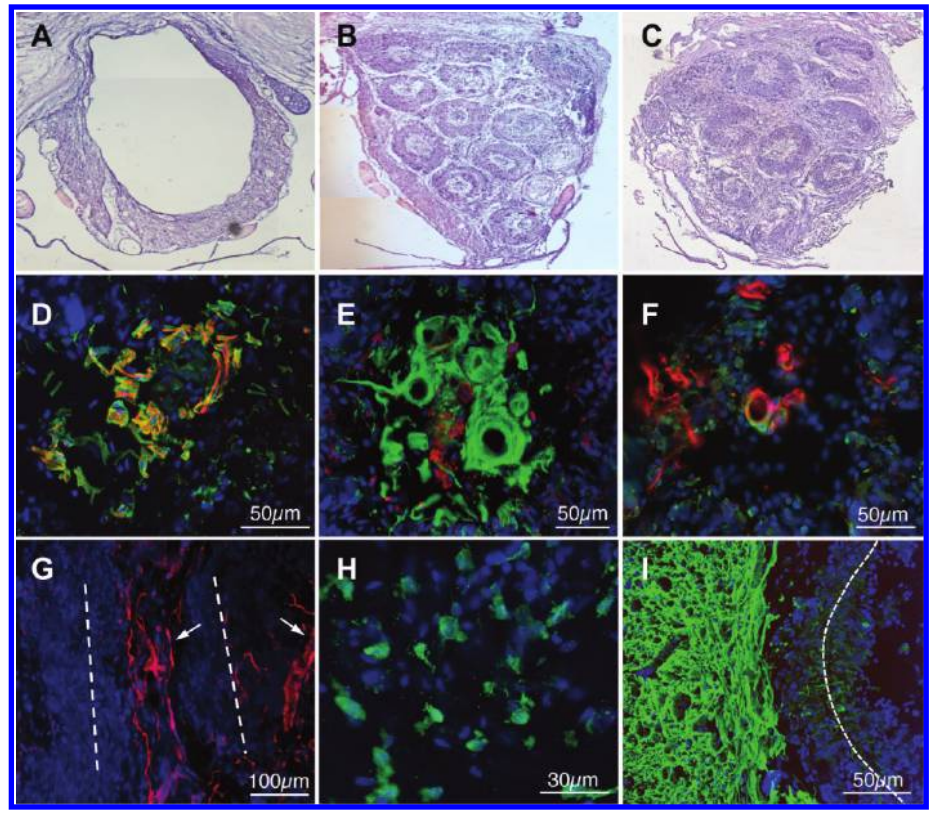

Figure 2. Histological and immunofluorescence analysis. Hematoxylin-eosin transverse spinal cord sections are shown, ventral side down, 6 months post-transplant. (A) A large cyst fills the large part of the lesion epicenter in sham-operated animals. In animals transplanted with guidance channels in groups 1 (B) and 2 (C), the cyst has been replaced by tissue-like material. Immunostainings of the inner lumens revealed NF200 positive fibers (red) surrounded by laminin deposits (green) (D), sporadic CD68 positive cells (red) (E), and abundant collagen IV deposition (in green) around the lumen of putative blood vessels. Networks of capillaries and vessels, positive for VWF, were detected (red) (F and G) adjacent to fibroblasts, the latter being located preferentially in the tube walls (F). Microglial cells were also detected inside the channels and their walls (H). GFAP positive cells (green) were found mainly outside the implants (I). Dashed lines outline guidance channel walls. Cell nuclei (DAPI; blue, D−I).

ologic levels (Figure 2H), also infiltrating the tube walls, indicating their involvement in the gradual scaffold biodegradation. Gliotic astroglial layers were occasionally found to surround the implants, while GFAP-positive cells were less frequent between the tubular channels and inside their lumens (Figure 2I).

Bridging the Spinal Cord Gap and Myelination. We asked if the observed anatomo-histological reconstruction resulted in axonal regeneration. While the SC of sham-operated animals showed only cyst cavities at the lesion site, quite extensive growth of regenerating fascicular nerve fibers was detected by anti-GAP43 immunolabeling,[43] within and among the implanted guidance conduits (Figure 3A). This was confirmed by the presence of numerous NF200- (group 2) and βIII-tubulin-positive fibers (groups 1 and 2), crossing both the proximal and distal lesion boundaries (Figure 3B and C). We quantified the percentage of guidance channels containing positive fibers for GAP43, βIII-tubulin, and NF200 throughout the whole conduit length, discounting those in which bridging was incomplete (Figure 3D). Within group 1 ($n = 5$), *i.e.*, animals implanted with guidance channels without GFs, 78.00 ± 10.92% of the channels tested positive for GAP-43, 37.64 ± 11.99% were βIII-tubulin-positive, and none contained fibers positive for NF200 throughout the lesion gap. Animals receiving both channels and GFs (group 2; $n = 8$) showed the highest percentage of fibers positive for all three markers: 100 ± 0% of the channels were positive for GAP-43; 92.83 ± 4.6% for βIII-tubulin, and 52.65 ± 15.3% for NF200. Statistical analysis showed a significant difference for both NF200 and βIII-tubulin ($p = 0.03$ and 0.003 respectively; Mann−Whitney rank sum test) in favor of animals receiving both channels and GFs, as compared to channels alone. No significant difference was found for GAP-43 ($p = 0.093$). As expected, anti-NF-200 staining did not colocalize with GAP43 immunofluorescence, although both kinds of fibers were often detected within the same tubes (Figure 3E). Of note, 18.03 ± 3.08% ($n = 5$) and 38.13 ± 5.84% ($n = 8$) of the fibers positive for βIII-tubulin were tightly associated with antimyelin basic protein (MBP) immunolabeling in groups 1 and 2, respectively (Figure 3F and enlargement in Figure 3G), suggesting that myelination of regenerating neuronal processes occurs within the implants. Finally, fibers positive for SMI-32 (Figure 3H)—the nonphosphorylated isoform of NF 200—were detected within guidance conduits, to-

gether with those stained by SMI-31 (Figure 3I), specific for phosphorylated NF200, all across the lesion and crossing into the tissue at both the distal and proximal interfaces. This shows the presence of both immature and mature axons and of myelination throughout the regenerating lesion area. Axonal regrowth, crossing both rostral and caudal implant/tissue interfaces, was aligned with tubular channel orientation (Figure 3J dashed lines).

In summary, the newly formed tissue comprised both stromal (fibroblasts, endothelium, and microglia) and neural parenchymal cells (astrocytes, neurons, and myelinating cells). Astrocytes were found between and around the degrading guidance channels together with neuronal fibers, myelin, microglial cells, fibroblasts, basement membrane components, and endothelial vessels. While the same cell types were also found inside the channels, the relative frequency of neurons and astroglia were quite different.

In turn, the greater majority of the tubes (>75%) contained thick bundles of neuronal fibers (GAP43 positive cells), cells located throughout the whole length of the microconduits, running along the longitudinal axis and crossing the tissue/conduit interfaces at both rostral and caudal ends. There was a significant difference in the composition of the neuronal fibers found within the guidance channels filled with SAPs and GFs as compared to those with SAPs alone, since the latter contained only GAP43- or βIII-tubulin positive fibers and in lesser amounts as compared to channels with GFs. The presence of GFs also led a significant fraction of the neuronal fibers to be labeled with the mature NF-200 neuronal marker, in good agreement with the presence of larger amounts of MBP than observed in channels without GFs (Figure 3F and G). This leads to infer the transplantation of guidance channels warrants, *per se*, not only the preservation of the cord anatomy but also the onset of significant axonal regeneration. Second the presence of pro-regenerative cytokines, which SAPs are known can release gradually,[29] supports the maturation of the neurons and their processes. The continued presence of both immature and mature neuronal processes inside the GF-containing channels, as long as six months after transplantation, shows that nerve regeneration is still active at this time. This and the fact that guidance channels are still being readsorbed suggests that the pro-regenerative effects of these composite neural prosthetics exceeds the six month end-point tested here. To the best of our knowledge, this is the first report describing the accomplishment of such a prominent level of anatomical restoration in substitution of the cysts in chronic SCI.

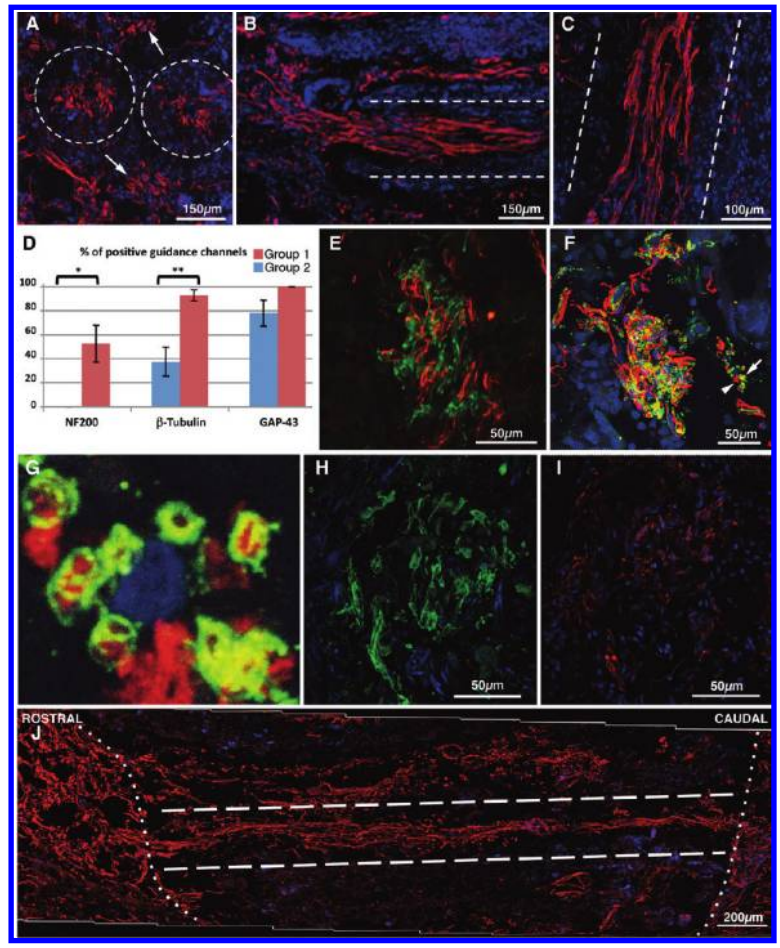

Figure 3. Nervous regeneration in the chronically injured rat SC. Dashed lines outline channel walls in (A−C). In transverse sections (A), GAP-43 positive fibers were found inside and between transplanted tubes (arrows; coronal section). (B) NF200 positive fibers were seen crossing the top rostral interface of the lesion. (C). βIII-tubulin positive fasciculi stretched through the lumen of the conduits in a longitudinal spinal cord section. (D) Quantitative analysis (mean ± SEM) of the percentage of channels showing positivity for neural markers throughout the entire tube length ($N = 5$ for group 1, $N = 8$ for group 8). Statistical significance: (*) $p = 0.03$; (**) $p = 0.003$. NF200 (green) and GAP43 (red) did not colocalize inside the same fiber (E). Myelinated (green, arrow) and unmyelinated (red, arrowhead) βIII-tubulin positive fibers (F) were observed (enlargement in G). Both SMI-32 (H) and SMI-31 (I) positive fibers were detected within guidance conduits, in adjacent coronal sections. In the longitudinal reconstruction of transplanted cord in (J) (group 2), NF200 positive fibers cover the whole length (approx 2 mm) of the lesion, crossing both the rostral and the caudal channels/tissue interfaces (dotted line).

Functional Recovery: BBB and Electrophysiological Analysis. The anatomical, histological, and neuronal regeneration observed in transplanted animals was accompanied by functional recovery. We evaluated motor function by means of serial BBB score analysis. At one week post-transplantation, the average BBB score was homogeneous between all experimental groups (Figure 4). Notably, significant differences gradually emerged between group 0 ($n = 10$) and groups 1 and 2 ($n = 11$ and 16, respectively). Animals in group 2, receiving guidance channels plus GFs, showed the best performance, with significantly improved BBB scores as compared to

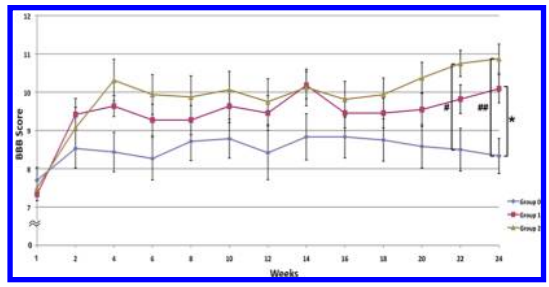

Figure 4. BBB scores of the experimental groups. BBB scores of animals in groups 0 ($N = 10$), 1 ($N = 11$), and 2 ($N = 16$). At weeks 22 (#) and 24 (##), BBB scores of group 2 differed significantly from group 0: $p = 0.005$ and $p < 0.001$, respectively, while group 1 reached statistical significance with respect to group 0 at week 24 (*): $p = 0.041$.

sham animals (group 0) at 22 and 24 weeks post-transplant ($p = 0.005$ and $p < 0.001$, respectively (one way Anova−Tukey test). Significant differences between groups 0 and 1 emerged at 24 weeks ($p = 0.041$).

Electrophysiological investigation was carried out to evaluate the transmission through ascending and descending pathways also in comparison to healthy animals. Descending responses evoked by epicortical stimulation are shown in Figure 5A and B. The muscular origin[44] was confirmed, and their source identified in the iliopsoas (IL) and quadratus lumborum (QL) muscles (Figure 5B) (see Methods Section). In all of the experimental groups (*i.e.*, group 0−2), amplitude of the maximum descending responses (Figure 5A) was about 10-fold smaller than in healthy animals. Notably, responses were larger in both groups receiving guidance channels, being the highest in group 1 and intermediate in group 2 as compared to the lowest score in group 0, although statistical significance was detected only between group 1 and 0 (two-way ANOVA, group main effect $F(2, 19) = 7.39$, $p < 0.005$; Tukey posthoc analysis $p < 0.004$). Also, ANOVA showed the responses to be significantly smaller in groups 0−2 than in healthy animals ($F(3, 24) = 73.86$, $p < 0.005$, posthoc $p < 0.0002$), whereas latency of spinal responses did not differ between the four groups (groups 0−2 and healthy animals) (global mean ± SD, 3.81 ±0.53 ms) (Figure 5B). Analysis of the amplitude of the maximum cortical responses evoked by epidural dorsal roots stimulation (Figure 5C,D) revealed both a group ($F(2, 20) = 4.19$, $p < 0.04$) and a side (left > right, $F(1, 20) = 23.57$, $p < 0.0001$) main effect, with no interactions, indicating that the side effect was distributed to all groups independently from the presence of the lesion. As for the descending responses, amplitude of the cortical responses was significantly larger in healthy than in lesioned animal groups 0−2 (group main effect $F(3, 25) = 9.02$, $p < 0.0003$; posthoc $p < 0.0003$, $p < 0.02$, $p < 0.005$ for comparisons with group 0−2, respectively). Again, within the lesion groups, the posthoc analysis showed that difference was significant only between group 1 and 0 ($p < 0.04$). The latency of the first positive (P1) peak of cortical potentials was significantly longer in lesioned animals in all groups 0−2 than in healthy rats (group main effect $F(3, 25) = 91.85$, $p < 0.00001$; posthoc, $p < 0.0002$). Notwithstanding, latency was significantly longer in group 0 than in animals receiving guidance channels in both group 1 and 2 (group main effect $F(2, 18) = 7.58$, $p < 0.005$, posthoc $p < 0.02$ and $p < 0.009$ for group 1 and 2 with respect to group 0) (Figure 5E and F). The P1−N1 time difference (duration of the ascending response) did not show any significant change between the 4 groups of animals.

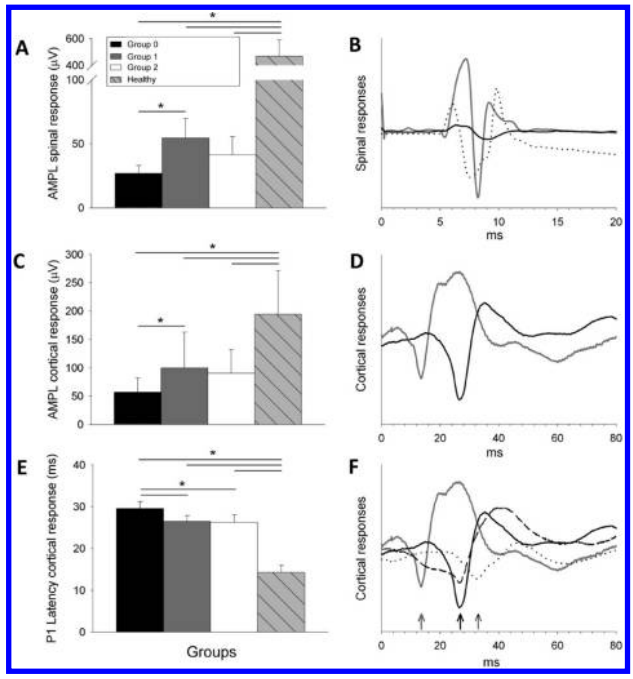

Figure 5. Electrophysiology tests. (A) Mean amplitude (±SD) of the maximum spinal responses evoked by epicortical stimulation. Among lesioned animals, responses are significantly larger in group 1 than in group 0. (B) Example of a maximum spinal response in one healthy (gray line) and in group 1 lesioned rat (black line). Dotted line shows the EMG response recorded in control experiments in the IL−QL muscles. (C) Mean amplitude (±SD) of the maximum cortical responses evoked by cauda equina dorsal roots epidural stimulation. Among lesioned animals, responses are significantly larger in group 1 than in group 0. (D) A maximum cortical response in one healthy (gray line) and one group 1 rat (black line). (E) Mean latency (±SD) of the first positive peak (P1) of cortical responses evoked by dorsal roots stimulation. (F) Example of a maximum cortical response in one healthy (gray line) and in group 0 (dotted line), group 1 (black line), and group 2 (dashed line) rats. Arrows mark P1 latency. Statistical significance: (*) $p < 0.05$.

Electrophysiological findings showed a significant amelioration in the amplitude of muscular responses likely evoked by activation of brain stem fast descending pathways, as suggested by the response conduction velocity, in rats receiving channels alone (Figure 5). Direct reinnervation of the motor neurons by axons regenerating through the scaffolds system remains possible, although unlikely, however more reasonable explanation implies that the observed axonal fiber regeneration occurred particularly in descending catecholaminergic systems with diffuse innervation,[45] known to modulate the excitability of spinal interneurones,[46] and motoneurons.[47] If so, those axons respon-

sible for the fast potential surviving the lesion might have acted on a progressively increasing number of excitable segmental neurons, thus evoking larger motor responses as regeneration proceeded. Accordingly, cortical sensory potential was significantly larger in transplanted than in sham-operated rats. Here the latency of cortical potentials was much longer in lesioned than in healthy rats with significant differences between sham operated and rats receiving guidance channels, suggesting a possible regeneration of ascending fibers across the lesion. Although the delayed cortical responses may be caused by unmasking of ascending transmission through ventral pathways spared by the lesion, the conjoint increase in amplitude and conduction velocity in transplanted animals suggests that neuro-prosthetics may support regeneration of injured axonal pathways.

CONCLUSIONS

In this work, we pursued the repair of the chronically injured SC[37] by attempting to replace the fluid-filled cyst found in these lesions with a neuro-prosthetics conducive to tissue reconstruction and axonal regeneration. Electrospun fibers and SAPs, assembled into composite hollow guidance channels, were transplanted into the cavity of chronic, postcontusive lesions of the thoracic SC, also in combination with pro-regenerative cytokines. Over a six month period, this resulted in significant anatomical reconstruction, by which the cyst was substituted with new nervous tissue, with axons and neural and stromal cells found both between the reabsorbing channels and inside them. In the large majority of the microconduits, the regenerating nerve fibers were detected throughout the whole channels' length, amidst a well-developed vascular network, basal lamina components, and myelin. This was matched by a significant improvement of both the electrophysiological activity of ascending and descending motor pathways and the locomotion score in the BBB test.

This work shows that a significant level of anatomical and functional regeneration can be accomplished in chronic injuries of the spinal cord by transplantation of multinanostructured composite scaffolds, under experimental settings that mimic the kind of lesion mostly affecting humans. Axonal regeneration is still active six months after transplant, showing that an even broader margin of improvement can be accomplished. Furthermore, electrospun fibers can be readily established from virtually any polymeric material, their diameters can be tuned at the micro- and nanoscale.[48] Thus, combining them in composite frames with SAPs offers the advantage of pre-establishing high surface area to volume ratio scaffolds. Given the overall high-density functionalization attainable with different bioactive motifs and the tunability of diffusive capacities to specific drugs[29] of SAPs, it is now possible to design biomimetic scaffolds with the specific mechanical and degradation properties required by neuro-prosthetics for the use in therapeutic applications.[37]

For all these reasons we propose this work as a prototypical study, providing the proof of principle that spatially guided regeneration in the chronically injured spinal cord can be accomplished by composite nanostructured scaffolds. Indeed, viewing our settings as a promising starting point, tomographic imaging of the cystic cavity and subsequent personalized nanostructured scaffold design, broader selection of cytokines that they may be engineered to release over time, prosthetic seeding with stem cells, and intensive rehabilitation are some of the increasingly complex and refined approaches that can be built, which will eventually lead to the development of effective experimental therapies in humans.

EXPERIMENTAL METHODS

Guidance Channels and Laminae Electrospinning. A 3:1 mixture of chloroform: methanol by volume was used to create an electrospinning solution of 5.5% poly(ε-caprolactone) (PCL, MW 80 000, Sigma-Aldrich) and 4% poly(DL-lactide-co-glycolide) (PLGA, 75:25, MW 66 000−107 000, Sigma-Aldrich) by weight. The electrospinning was performed using a parallel plate apparatus, as described previously.[48] Spinal cord guidance microtubes were synthesized by depositing electrospun fibers on grounded 4 cm 33G microneedles with an outer diameter of 210 μm (Hamilton) for 20 s. Fibers were deposited but actually did not adhere to the microneedles. Needles were rotated during fiber deposition in order to ensure uniform coating. To create the sealing lamina, PCL/PLGA nanofibers were deposited on a flat surface for 20 min and then were annealed for 24 h at 55 °C under vacuum to remove any possible residual solvent. See Supporting Information for SEM characterization of channels. End-on images were used to measure tube diameter and wall thickness.

SAPeptide Synthesis and Purification. The self-assembling peptide RADA16-I-BMHP1 (Ac-RADARADARADARADAGGPFSSTKT-CONH2) was F-moc synthesized *via* a Liberty microwave automated synthesizer (CEM). Sample masses were verified *via* a matrix-assisted laser desorption/ionization time-of-flight (MALDI-TOF) mass spectrometer (Applied biosystems), HPLC purified (Waters), and lyophilized (Labconco). Final purity was >95%. Samples were dissolved, and SEM was characterized, as described in Supporting Information.

Surgery and Animal Care. All procedures involving animals were performed according to EC guidelines (EC Council Directive 86/609, 1987), to the Italian legislation on animal experimentation (Decreto L. vo 116/92) and to protocols approved by the Animal Care and Use Committee of the University of Milan-Bicocca (IACUC 37/07). Female Sprague−Dawley rats underwent a laminectomy. Surgeries were performed *via* an OPMI-pico surgical microscope (Zeiss). A 2 cm longitudinal skin incision was centered over the T9-T10 spinous process along the midline. Without disrupting the *dura mater*, the tenth thoracic (T10) spinal segment was exposed by removing the dorsal part of the vertebra. The medial and ventral parts of the vertebra, spared by the surgery, allowed for weight support, thus not requiring the implantation of an additional osteosynthesis device. The exposed cord was contused by a 10 gr weight dropped from a height of 25 mm by using a MASCIS impactor device (Rutgers University). The impact velocity and compression were monitored and recorded to

guarantee consistency between animals. After injury, the muscles were sutured and the skin was closed with wound clips. After four weeks, when approximately 76% of the injured rats had survived, animals were randomly divided into three main experimental groups. After re-exposure of the lesioned spinal cord, meninges were incised, scar tissue and debris were removed *via* myelotomy, and saline solution was added (Group O, $N = 15$). Following scar tissue removal, groups 1 and 2 were submitted to the insertion of 10−13 electrospun tubes of 2−3 mm length. PBS-soaked tubes were easily peeled off the needles *via* surgical forceps. In group 1 ($N = 16$) the guidance channels were filled only with RADA16-I-BMHP1. In group 2 ($N = 24$) RADA16-I-BMHP1 was mixed with the following growth factors: brain-derived neurotrophic factor (1 mg/mL) and ciliary neurotrophic factor (1 mg/mL), both involved in neuronal development, survival, outgrowth, and neural regeneration *in vivo*;[32] vascular endothelial growth factor (1 mg/mL), capable of promoting angiogenesis;[31] and chondroitinase ABC (60 mU/μL), proven to remove the side chains of chondroitin sulfate proteoglycans in the gliotic scar.[7]

Special attention was focused on avoiding tube collapse by holding wetted channels in place with one or both forcep braces and positioned tubes by gently placing them one by one along the longitudinal SC axis and constructing a horizontal layer at the time. Four layers of tubes were usually necessary to fill the debrided injury site. The electrospun lamina positioned over the injury site was sutured with the *dura mater*. Animals were monitored for autophagia, and the bladders were expressed manually until voiding reflexes were re-established. See Supporting Information for a detailed description of the protocol.

Behavioral Analysis. Recovery of hind limb stepping movements in injured rats was evaluated using the Basso, Beattie, and Bresnahan (BBB) open-field locomotor test at 1 week after treatment and, subsequently, every two weeks.[34] Animals were blind-tested individually in an open-field testing area independently by two operators and were video-monitored with a digital camera. BBB scores, ranging from 0 (no hind limb movement) to 21 (coordinated gait with parallel paw placement), reflect combinations of rat hindlimb movements, trunk position and stability, stepping, coordination, paw placement, toe clearance, and tail position, representing sequential recovery stages that rats attain after SCI.

Immunohistochemistry. Twenty-four weeks after the second surgery, rats were perfused. The spinal cords were dissected, post-fixed for 4 h in 4% paraformaldehyde and cryoprotected in 30% sucrose overnight. Transverse or longitudinal sections underwent morphological evaluation *via* hematoxylin-eosin staining or fluorescence analysis *via* immunostainings for the following markers: antineurofilament NF200 (Sigma-Aldrich) for axons; anti-SMI-32 and anti-SMI-31 (Covance) to detect the unphosphorylated and phosphorylated isoforms, respectively, of the heavy subunit of neurofilament; anti-βIII-tubulin (Covance) for neurons; antimyelin basic protein (MBP) (Sternberger Monoclonals Incorporated) for myelin; antigrowth associated protein GAP-43 (Chemicon International) for growth cones and regenerating nerve fibers; anti-β P4HB for fibroblasts (Acris); anti-Von Willebrand factor VWF for endothelial cells (Dako); antiglial fibrillary acidic protein GFAP (Chemicon International) for astrocytes; antilaminin (Sigma-Aldrich) and antirat collagen IV (Cedarlene) as main components of the basal lamina in nervous tissue; anti-CD68 (Serotec) for macrophages; and anti-Iba-I (Wako) for microglia and macrophages. See more details in the Supporting Information. In transverse sections of spinal cord groups 1 and 2, we quantified the percentage of electrospun tubes infiltrated with fibers stained positive for nerve markers throughout the entire length of the conduit. βIII-tubulin positive fibers and MBP-wrapped fibers located in the inner lumen of 10 randomly chosen guidance channels were counted. Total MBP positive fibers were expressed as a percentage of the total βIII-tubulin positive fibers for each animal, and values were then averaged for animals belonging to the same experimental group.

Electrophysiology. Electrophysiological investigation was performed in 13 lesioned rats belonging to group 0 ($N = 4$), group 1 ($N = 4$), and group 2 ($N = 5$). The same testing was also performed on five control healthy rats. See Supporting Information for a detailed description of the adopted methodology. Experimenters were blind to the treatment each animal had received. L2−L3 vertebrae were exposed. One Ag Teflon-insulated wire (bare diameter 200 μm, coated 280 μm, A-M System Carlsborg) exposed at the cathode was introduced through the L2−L3 yellow ligament into the epidural space and referenced to an anode, tight to the spinous process of L3. These electrodes, placed in order to stimulate the cauda equina dorsal roots, also allowed recording of volume conducted muscle potentials.[44] Muscles originating these potentials were identified by this group in separate experiments as IL and QL, excluding a possible origin from more rostral epiaxial muscles. Holes were drilled bilaterally in the exposed skull in correspondence to the sensory motor cortex (±3 mm antero-posterior, 2.5 mm lateral from BREGMA) *via* a stereotaxic frame (Kopf Instruments). Through these holes, the exposed tips of Ag Teflon-insulated wire were placed over the *dura* and cemented in place. Additionally, Ag Teflon-insulated wire electrodes were inserted into the left splenium capitis (SC) and in the right and left biceps femoris (BF) muscles. As to epicortical stimulation, under general anesthesia, single stimuli (0.05 ms duration, interstimuls interval 7 s) were delivered over the sensory motor cortex through the extradural electrodes (impedance 40/60 KΩ, cathode at sensory cortex site, anode at motor site). Both hemispheres were tested in separate trials. See Supporting Information for a detailed description of the motivations triggering the developed technique. Descending responses induced by the stimulus were recorded simultaneously from the cervical and the hindlimb intramuscular electrodes in SC and BF and from the epidural electrode at the L2−L3 site. The fastest response recorded in SC muscle, located above the lesion, was used to control on each rat the efficacy of epicortical stimulation. Signals were amplified, filtered (1 Hz−3kHz), and A/D converted (sampling rate 5kHz). The stimulus intensity was varied in consecutive steps (range 1−4 mA) from threshold to the intensity that saturated the amplitude of the response recorded at the spinal site. Five responses were recorded and averaged for each intensity. For spinal cord stimulations, double stimuli (0.05 ms duration, 3 ms apart) were delivered from the epidural electrode, eliciting ascending evoked potentials in the sensory motor cortex of both hemispheres. Signals were amplified, filtered (1 Hz−3kHz), and A/D converted (sampling rate 5kHz). The stimulus intensity was varied in steps from threshold to the intensity saturating the amplitude of the cortical response (range 0.1−0.3 mA). Ten responses were averaged for each intensity. For each animal and stimulus intensity we measured: (i) the latency and peak-to-peak amplitude of the spinal descending responses and (ii) the latency of the first positive (P1) and first negative (N1) peaks and the P1−N1 peak-to-peak amplitude of the cortical evoked potentials.

Statistical Analysis. Data were processed using SigmaStat 3.1 software (Systat Software Inc.). Values are reported as mean ± SEM. Significance analysis of the percentage of positive microconduits between group 1 and group 2 was performed *via* Mann−Whitney rank sum test, and values were considered significantly different for $P < 0.05$. BBB score significance tests among groups were performed by one-way ANOVA and pairwise Tukey. Scores were considered significantly different for $P < 0.05$. As for electrophysiology data, a two-way ANOVA (factors: experimental group *vs* side) was used to compare the amplitude and the latency of the maximal descending responses obtained by cortical stimulation as well as the amplitude and latency of the ascending responses. All analyses were two-tailed and $P < 0.05$ were considered as statistically significant. *Post hoc* analysis was performed with the Tukey's HSD test for unequal number of samples.

Acknowledgment. We gratefully thank CARIPLO foundation, Regione Lombardia and the Nicholas G. and Dorotha K. Dumbros Scholarship and Fellowship Fund for providing financial support to the project.

Supporting Information Available: Figure S1 and Supplementary Methods. This material is available free of charge *via* the Internet at http://pubs.acs.org.

REFERENCES AND NOTES

1. Bunge, R. P.; Puckett, W. R.; Becerra, J. L.; Marcillo, A.; Quencer, R. M. Observations on the Pathology of Human Spinal Cord Injury. A Review and Classification of 22 New Cases with Details from a Case of Chronic Cord Compression with Extensive Focal Demyelination. *Adv. Neurol.* **1993**, *59*, 75–89.
2. Crowe, M. J.; Bresnahan, J. C.; Shuman, S. L.; Masters, J. N.; Beattie, M. S. Apoptosis and Delayed Degeneration after Spinal Cord Injury in Rats and Monkeys. *Nat. Med.* **1997**, *3*, 73–6.
3. Bunge, M. B. Bridging Areas of Injury in the Spinal Cord. *Neuroscientist* **2001**, *7*, 325–39.
4. Fawcett, J. W. The Glial Response to Injury and Its Role in the Inhibition of Cns Repair. *Adv. Exp. Med. Biol.* **2006**, *557*, 11–24.
5. Chan, C. C. Inflammation: Beneficial or Detrimental after Spinal Cord Injury. *Recent Pat. CNS Drug Discovery* **2008**, *3*, 189–99.
6. Neumann, S.; Bradke, F.; Tessier-Lavigne, M.; Basbaum, A. I. Regeneration of Sensory Axons within the Injured Spinal Cord Induced by Intraganglionic Camp Elevation. *Neuron* **2002**, *34*, 885–93.
7. Bradbury, E. J.; Moon, L. D.; Popat, R. J.; King, V. R.; Bennett, G. S.; Patel, P. N.; Fawcett, J. W.; McMahon, S. B. Chondroitinase Abc Promotes Functional Recovery after Spinal Cord Injury. *Nature* **2002**, *416*, 636–40.
8. Kwon, B. K.; Liu, J.; Messerer, C.; Kobayashi, N. R.; McGraw, J.; Oschipok, L.; Tetzlaff, W. Survival and Regeneration of Rubrospinal Neurons 1 Year after Spinal Cord Injury. *Proc. Natl. Acad. Sci. U.S.A.* **2002**, *99*, 3246–51.
9. Pallini, R. Anatomy Of "Regenerating Axons. *Science* **1998**, *280*, 181–2.
10. Bareyre, F. M.; Schwab, M. E. Inflammation, Degeneration and Regeneration in the Injured Spinal Cord: Insights from DNA Microarrays. *Trends Neurosci.* **2003**, *26*, 555–63.
11. Fouad, K.; Schnell, L.; Bunge, M. B.; Schwab, M. E.; Liebscher, T.; Pearse, D. D. Combining Schwann Cell Bridges and Olfactory-Ensheathing Glia Grafts with Chondroitinase Promotes Locomotor Recovery after Complete Transection of the Spinal Cord. *J. Neurosci.* **2005**, *25*, 1169–78.
12. Watanabe, K.; Nakamura, M.; Iwanami, A.; Fujita, Y.; Kanemura, Y.; Toyama, Y.; Okano, H. Comparison between Fetal Spinal-Cord- and Forebrain-Derived Neural Stem/Progenitor Cells as a Source of Transplantation for Spinal Cord Injury. *Dev. Neurosci.* **2004**, *26*, 275–87.
13. Ramer, M. S.; Priestley, J. V.; McMahon, S. B. Functional Regeneration of Sensory Axons into the Adult Spinal Cord. *Nature* **2000**, *403*, 312–6.
14. Shapiro, S.; Borgens, R.; Pascuzzi, R.; Roos, K.; Groff, M.; Purvines, S.; Rodgers, R. B.; Hagy, S.; Nelson, P. Oscillating Field Stimulation for Complete Spinal Cord Injury in Humans: A Phase 1 Trial. *J. Neurosurg. Spine* **2005**, *2*, 3–10.
15. Engesser-Cesar, C.; Anderson, A. J.; Basso, D. M.; Edgerton, V. R.; Cotman, C. W. Voluntary Wheel Running Improves Recovery from a Moderate Spinal Cord Injury. *J. Neurotrauma* **2005**, *22*, 157–71.
16. Takami, T.; Oudega, M.; Bates, M. L.; Wood, P. M.; Kleitman, N.; Bunge, M. B. Schwann Cell but Not Olfactory Ensheathing Glia Transplants Improve Hindlimb Locomotor Performance in the Moderately Contused Adult Rat Thoracic Spinal Cord. *J. Neurosci.* **2002**, *22*, 6670–81.
17. Kadoya, K.; Tsukada, S.; Lu, P.; Coppola, G.; Geschwind, D.; Filbin, M. T.; Blesch, A.; Tuszynski, M. H. Combined Intrinsic and Extrinsic Neuronal Mechanisms Facilitate Bridging Axonal Regeneration One Year after Spinal Cord Injury. *Neuron* **2009**, *64*, 165–72.
18. Karimi-Abdolrezaee, S.; Eftekharpour, E.; Wang, J.; Schut, D.; Fehlings, M. G. Synergistic Effects of Transplanted Adult Neural Stem/Progenitor Cells, Chondroitinase, and Growth Factors Promote Functional Repair and Plasticity of the Chronically Injured Spinal Cord. *J. Neurosci.* **2010**, *30*, 9.
19. Schreyer, D. J.; Jones, E. G. Growth of Corticospinal Axons on Prosthetic Substrates Introduced into the Spinal Cord of Neonatal Rats. *Brain Res.* **1987**, *432*, 291–9.
20. Tsai, E. C.; Dalton, P. D.; Shoichet, M. S.; Tator, C. H. Matrix Inclusion within Synthetic Hydrogel Guidance Channels Improves Specific Supraspinal and Local Axonal Regeneration after Complete Spinal Cord Transection. *Biomaterials* **2006**, *27*, 519–33.
21. Teng, Y. D.; Lavik, E. B.; Qu, X.; Park, K. I.; Ourednik, J.; Zurakowski, D.; Langer, R.; Snyder, E. Y. Functional Recovery Following Traumatic Spinal Cord Injury Mediated by a Unique Polymer Scaffold Seeded with Neural Stem Cells. *Proc. Natl. Acad. Sci. U.S.A.* **2002**, *99*, 3024–9.
22. Oudega, M.; Gautier, S. E.; Chapon, P.; Fragoso, M.; Bates, M. L.; Parel, J. M.; Bunge, M. B. Axonal Regeneration into Schwann Cell Grafts within Resorbable Poly(Alpha-Hydroxyacid) Guidance Channels in the Adult Rat Spinal Cord. *Biomaterials* **2001**, *22*, 1125–36.
23. Deumens, R.; Koopmans, G. C.; Honig, W. M.; Maquet, V.; Jerome, R.; Steinbusch, H. W.; Joosten, E. A. Chronically Injured Corticospinal Axons Do Not Cross Large Spinal Lesion Gaps after a Multifactorial Transplantation Strategy Using Olfactory Ensheathing Cell/Olfactory Nerve Fibroblast-Biomatrix Bridges. *J. Neurosci. Res.* **2006**, *83*, 811–20.
24. Cai, J.; Ziemba, K. S.; Smith, G. M.; Jin, Y. Evaluation of Cellular Organization and Axonal Regeneration through Linear Pla Foam Implants in Acute and Chronic Spinal Cord Injury. *J. Biomed. Mater. Res., Part A* **2007**, *83*, 512–20.
25. Gelain, F. Novel Opportunities and Challenges Offered by Nanobiomaterials in Tissue Engineering. *Int. J. Nanomed.* **2008**, *3*, 415–24.
26. Li, W. J.; Mauck, R. L.; Cooper, J. A.; Yuan, X.; Tuan, R. S. Engineering Controllable Anisotropy in Electrospun Biodegradable Nanofibrous Scaffolds for Musculoskeletal Tissue Engineering. *J. Biomech.* **2007**, *40*, 1686–93.
27. Ellis-Behnke, R. G.; Liang, Y. X.; You, S. W.; Tay, D. K.; Zhang, S.; So, K. F.; Schneider, G. E. Nano Neuro Knitting: Peptide Nanofiber Scaffold for Brain Repair and Axon Regeneration with Functional Return of Vision. *Proc. Natl. Acad. Sci. U.S.A.* **2006**, *103*, 5054–9.
28. Prabhakaran, M. P.; Venugopal, J.; Chyan, T. T.; Hai, L. B.; Chan, C. K.; Tang, A. L.; Ramakrishna, S. Electrospun Biocomposite Nanofibrous Scaffolds for Neural Tissue Engineering. *Tissue Eng., Part A* **2008**, .
29. Gelain, F.; Unsworth, L. D.; Zhang, S. Slow and Sustained Release of Active Cytokines from Self-Assembling Peptide Scaffolds. *J. Controlled Release* **2010**, *145*, 231–239.
30. Gelain, F.; Bottai, D.; Vescovi, A.; Zhang, S. Designer Self-Assembling Peptide Nanofiber Scaffolds for Adult Mouse Neural Stem Cell 3-Dimensional Cultures. *PLoS One* **2006**, *1*, e119.
31. Wilcke, I.; Lohmeyer, J. A.; Liu, S.; Condurache, A.; Kruger, S.; Mailander, P.; Machens, H. G. Vegf(165) and Bfgf Protein-Based Therapy in a Slow Release System to Improve Angiogenesis in a Bioartificial Dermal Substitute in Vitro and in Vivo. *Langenbecks Arch. Surg.* **2007**, *392*, 305–14.
32. Storer, P. D.; Dolbeare, D.; Houle, J. D. Treatment of Chronically Injured Spinal Cord with Neurotrophic Factors Stimulates Betaii-Tubulin and Gap-43 Expression in Rubrospinal Tract Neurons. *J. Neurosci. Res.* **2003**, *74*, 502–11.
33. Radojicic, M.; Nistor, G.; Keirstead, H. S. Ascending Central Canal Dilation and Progressive Ependymal Disruption in a Contusion Model of Rodent Chronic Spinal Cord Injury. *BMC Neurol.* **2007**, *7*, 30.
34. Basso, D. M.; Beattie, M. S.; Bresnahan, J. C.; Anderson, D. K.; Faden, A. I.; Gruner, J. A.; Holford, T. R.; Hsu, C. Y.; Noble, L. J.; Nockels, R.; et al. Mascis Evaluation of Open Field Locomotor Scores: Effects of Experience and Teamwork on Reliability. Multicenter Animal Spinal Cord Injury Study. *J. Neurotrauma* **1996**, *13*, 343–59.

35. Norenberg, M. D.; Smith, J.; Marcillo, A. The Pathology of Human Spinal Cord Injury: Defining the Problems. *J. Neurotrauma* **2004**, *21*, 429–40.
36. Bamber, N. I.; Li, H.; Aebischer, P.; Xu, X. M. Fetal Spinal Cord Tissue in Mini-Guidance Channels Promotes Longitudinal Axonal Growth after Grafting into Hemisected Adult Rat Spinal Cords. *Neural Plast.* **1999**, *6*, 103–21.
37. Novikova, L. N.; Novikov, L. N.; Kellerth, J. O. Biopolymers and Biodegradable Smart Implants for Tissue Regeneration after Spinal Cord Injury. *Curr. Opin. Neurol.* **2003**, *16*, 711–5.
38. Sun, H.; Mei, L.; Song, C.; Cui, X.; Wang, P. The in Vivo Degradation, Absorption and Excretion of Pcl-Based Implant. *Biomaterials* **2006**, *27*, 1735–40.
39. Gelain, F.; Lomander, A.; Vescovi, A. L.; Zhang, S. Systematic Studies of a Self-Assembling Peptide Nanofiber Scaffold with Other Scaffolds. *J. Nanosci. Nanotechnol.* **2007**, *7*, 424–34.
40. Koh, H. S.; Yong, T.; Chan, C. K.; Ramakrishna, S. Enhancement of Neurite Outgrowth Using Nano-Structured Scaffolds Coupled with Laminin. *Biomaterials* **2008**, *29*, 3574–82.
41. Georges, P. C.; Miller, W. J.; Meaney, D. F.; Sawyer, E. S.; Janmey, P. A. Matrices with Compliance Comparable to That of Brain Tissue Select Neuronal over Glial Growth in Mixed Cortical Cultures. *Biophys. J.* **2006**, *90*, 3012–8.
42. Anderson, C. R.; Ashwell, K. W. S.; Collewijn, H.; Conta, A.; Harvey, A.; Heise, C.; Hodgetts, S.; Holstege, G.; Kayalioglu, G.; Keast, J. R. *The Spinal Cord*; Academic Press: London, 2009.
43. Skene, J. H.; Willard, M. Axonally Transported Proteins Associated with Axon Growth in Rabbit Central and Peripheral Nervous Systems. *J. Cell Biol.* **1981**, *89*, 96–103.
44. Zileli, M.; Schramm, J. Spinal and Muscular Evoked Response Following Single Stimulation of the Motor Cortex of the Rat. *EEG EMG Z. Elektroenzephalogr. Elektromyogr. Verwandte Geb.* **1989**, *20*, 106–11.
45. Bjorklund, A. S. G. *Descending Monoaminergic Projections to the Spinal Cord*; Biomedical Press: Amsterdam, The Netherlands, 1982.
46. Hammar, I.; Stecina, K.; Jankowska, E. Differential Modulation by Monoamine Membrane Receptor Agonists of Reticulospinal Input to Lamina Viii Feline Spinal Commissural Interneurons. *Eur. J. Neurosci.* **2007**, *26*, 1205–12.
47. Hultborn, H.; Brownstone, R. B.; Toth, T. I.; Gossard, J. P. Key Mechanisms for Setting the Input-Output Gain across the Motoneuron Pool. *Prog. Brain Res.* **2004**, *143*, 77–95.
48. Fridrikh, S. V.; Yu, J. H.; Brenner, M. P.; Rutledge, G. C. Controlling the Fiber Diameter During Electrospinning. *Phys. Rev. Lett.* **2003**, *90*, 144502.